https://doi.org/10.5194/egusphere-2023-238
Preprint. Discussion started: 3 April 2023

Stochastic properties of coastal flooding events – Part 2: Probabilistic analysis

Byungho Kang[1,2], Rusty A. Feagin[3,1,*], Thomas Huff[3,*], and Orencio Durán Vinent[1]

[1]Department of Ocean Engineering, Texas A&M University, College Station, TX, USA
[2]Present address: Department of Civil and Environmental Engineering, University of Houston, Houston, TX, USA
[3]Department of Ecology and Conservation Biology, Texas A&M University, College Station, TX, USA
[*]These authors contributed equally to this work.

Correspondence: Orencio Durán Vinent (oduranvinent@tamu.edu)

Abstract. Low-intensity but high-frequency coastal flooding, also known as nuisance flooding, can negatively affect low-lying coastal communities with potentially large socioeconomic effects. This flooding also can greatly affect post-storm coastal dune recovery and reduce the long-term resilience of the back-barrier ecosystem. Recent analytical work has hypothesized that these frequent flooding events are uncorrelated in time and can be modeled as a marked Poisson process with exponentially distributed sizes, a result with important implications for the prediction of coastal flooding. Here we test this proposition using high-temporal-resolution field measurements of an eroding beach on the Texas coast. A time series of the flooded area was obtained from pictures using Convolutional Neural Network (CNN)-based semantic segmentation methods. After defining the flooding events using a peak-over-threshold method, we found that the size of the flooding events indeed followed an exponential distribution as hypothesized. Furthermore, the flooding events were uncorrelated with one another at daily time scales, but correlated at hourly time scales. Finally, we found relatively good statistical agreement between our CNN-based empirical flooding data and run-up predictions. Our results formalize the first probabilistic model of coastal flooding events driven by wave run-up which can be used in coastal risk management and landscape evolution models.

1 Introduction

Most coastal flooding is induced by a short-term rise in water levels caused by a mix of stochastic and deterministic events such as storm surges, wave runup, tides or river discharge due to heavy precipitation (Muis et al., 2016; Ward et al., 2018; Bevacqua et al., 2019). In addition to the extreme coastal flooding events with return periods in the order of ten or more years, the importance of low-intensity high-frequency coastal flooding, with return periods in the order of months, has recently became clear. When accumulated over time, the social cost of nuisance flooding can outweigh the costs from the large-scale flooding (Kriebel David and Dean Robert, 1993; Moftakhari et al., 2018). This low-intensity flooding also control the formation and post-storm recovery of coastal dunes, which are essential for the stability of barrier islands (Durán Vinent et al., 2021).

Recently, Rinaldo et al. (2021) studied the stochastic properties of high-water events associated with coastal flooding on a beach, defined as cluster of consecutive days when total water levels exceeded a given threshold. In this work, the total water level was calculated by adding the still water level from a buoy dataset to the wave runup estimated from an empirical

https://doi.org/10.5194/egusphere-2023-238
Preprint. Discussion started: 3 April 2023

formula based on the deep-water significant wave height and wavelength (Stockdon et al., 2006, 2014). They found that the high-water events overtopping the beach (i.e. flooding events) were uncorrelated and occurred randomly in time; by definition, these events can be modeled as a Poisson process. They also found that the size and intensity of an event, defined by the maximum total water level during the event, does not vary with increasing elevation. Given the empirical nature of the wave runup model underpinning the data, which does not take into account the detailed onshore wave propagation nor the varying nearshore profile, the stochastic properties outlined by Rinaldo et al. (2021) were only as good as the quality of the wave runup predictions.

In the present study, we aim to test the predictions made by Rinaldo et al. (2021) by applying the same peak-over-threshold technique to a high-resolution time series of camera images captured at a beach site on the Texas coast. The image analysis was done using Convolution Neural Network (CNN)-based image segmentation as explained in a companion contribution to this journal volume (Kang et al., in review). In the present study, we introduce and correct the time series of water data; define flooding events; perform the statistical analysis of both the size and inter-arrival of flooding events, and finally compare it to the results of Rinaldo et al. (2021).

2 Defining and measuring flooding events

2.1 Field data

As explained in a companion contribution to this journal volume (Kang et al., in review), we installed three solar-powered stationary GoPro cameras, each with a different field of view, on a beach near Cedar Lakes, Texas to monitor recovery after Hurricane Harvey in 2017. This site is subject to frequent wave runup events due to its low-lying, yet complex, bathymetric-topographic profile. Each camera captured pictures every 5 minutes during a 6 A.M–6 P.M. observation period and turned off automatically during the night. From November 2017 to May 2018, we captured more than 51,000 images.

2.2 Time series of water area fraction

In Kang et al. (in review), we applied CNN-based image segmentation to identify water pixels with an accuracy of more than 90%. Here we use the CNN to generate a time series of the number of water pixels from 24,793 consecutive non-overlapping daylight pictures, while filling the non-observation periods with zeros. For convenience, the number of water pixels was normalized by the total number of pixels in an image to obtain a water area fraction A(t) (Fig. 1). Since our observation period was about six months, we ignored the effect of seasonality and only corrected the images to account for three camera rotation events . These events were relatively mild in the angle of deflection, but were due to relatively strong winds. We also corrected for a change in position following one camera replacement on March 12th. These four changes of the camera field-of-view led to different base levels of water area fraction during non-flooding conditions (Fig. 2A). We identified this base level as the most probable value of the water area between camera rotations (or replacements) and thus estimated it from the mode of the water area distribution during that time period (Fig. 3). We then subtracted the base level(horizontal

https://doi.org/10.5194/egusphere-2023-238
Preprint. Discussion started: 3 April 2023

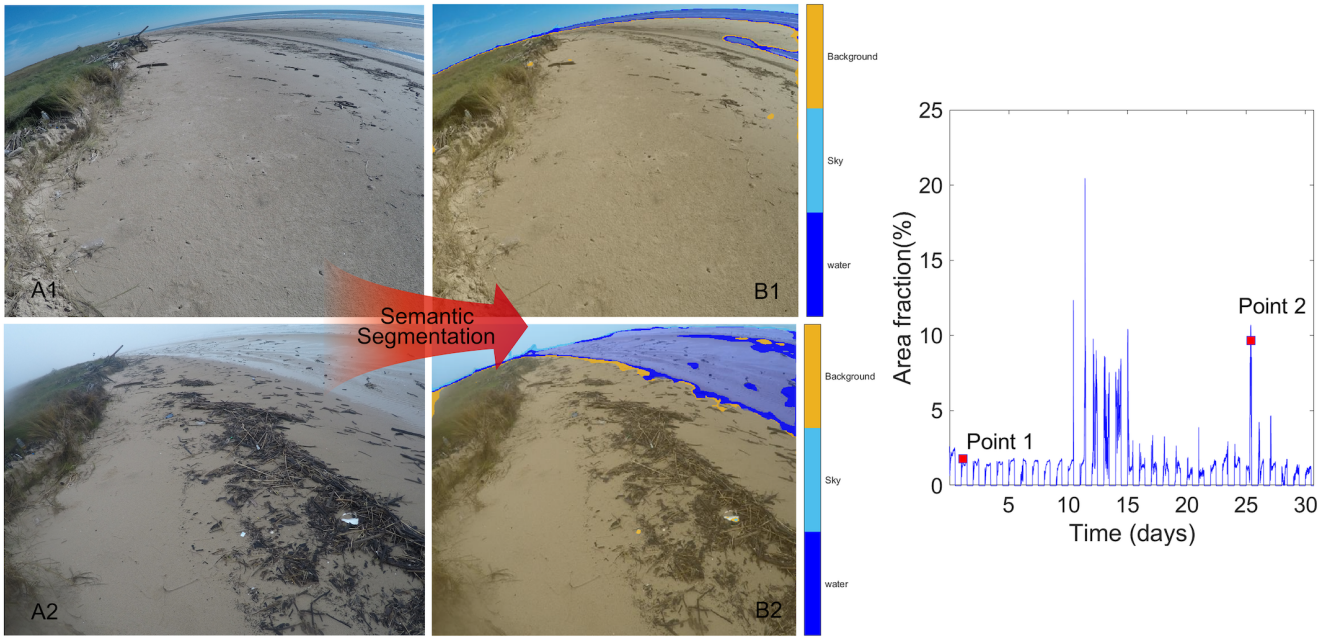

Figure 1. (A) Examples of non-flooding and flooding images captured from the camera. Two points at November 26th, 2017, 17:29 (point 1) and December 4th, 2017, 16:49 (point 2) are selected to illustrate the area fraction extraction process. (B) Semantic segmentation results using the convolutional neural network. Area fraction of the water region is based on the number of water-labeled pixels. (C)The illustration of the time series generation is based on water area fraction calculation using the captured images from November 23rd to December 23rd, 2017.

lines in Fig. 2) from $A(t)$ to obtain the excess water area fraction (Fig. 2B). We used $A(t)$ to denote the time series of this excess water area fraction. In order to study the stochastic properties of flooding events at different timescales, we found the time series of water area $A|_\tau(t)$ at the timescale τ, by taking the maximum of $A(t)$ over a time window τ. For example, $A|_{1\mathrm{h}}$ corresponded to an hourly time series, $A|_{1\mathrm{d}}$ to a daily time series, etc. Note that by definition, $A|_{5\mathrm{min}}$ was equivalent to $A(t)$ as pictures were taken every 5 minutes.

2.3 Definition of flooding events

We defined a flooding event as the set of consecutive values of the water area fraction $A|_\tau(t)$ that exceeded the 2% threshold (Fig. 4). This threshold was about twice the standard deviation of the water area distribution (Fig. 3) and allowed a clear separation between typical fluctuations in water area and the extreme events that characterized flooding conditions. From the definition, flooding events depended on the time window τ, as the consecutive threshold crossings at the sub-hour timescale merged at the daily timescale (Fig. 4).

Following Rinaldo et al. (2021), we characterized a flooding event i (for a given τ) by its starting time t_i, i.e. the time water area increased above 2%, its duration d_i, and its size S_i, defined as the maximum water area relative to the 2% threshold during

https://doi.org/10.5194/egusphere-2023-238
Preprint. Discussion started: 3 April 2023

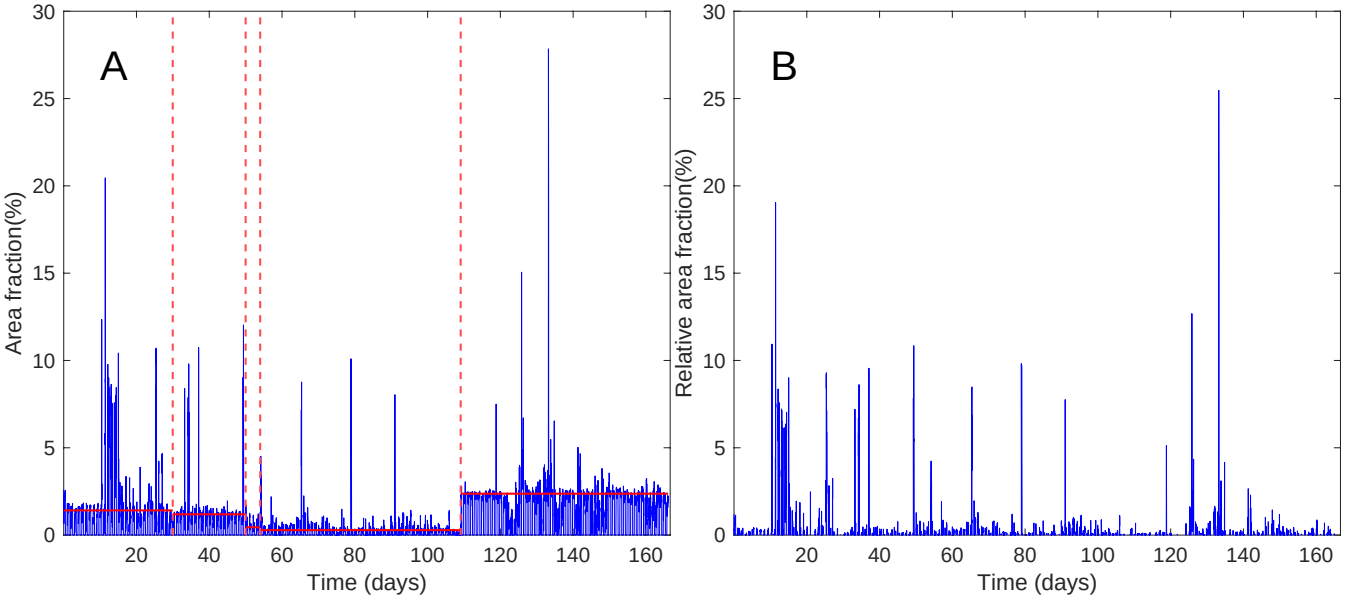

Figure 2. (A) Time series of original water area fraction. Red dashed lines indicate the camera rotation and replacement points that separate each time series segment, while solid lines show the offsets for each time segment. (B) Time series of the excess water area fraction $A(t)$ after deducting the offset (negative values were neglected).

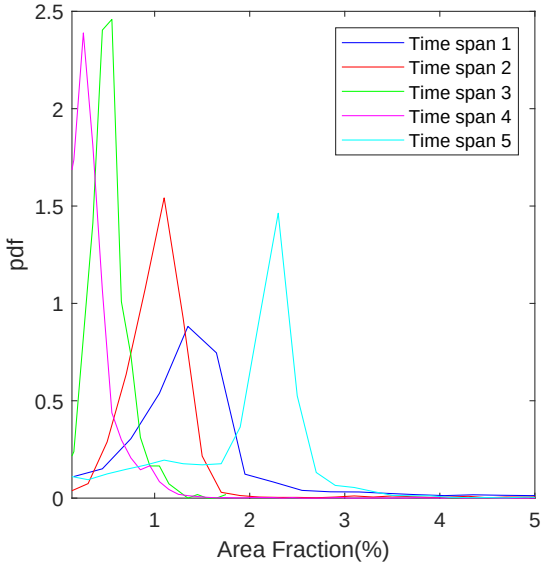

Figure 3. Probability density function (PDF) of water area fractions for each time spans in between camera rotations and/or replacements (see Fig. 2A).

https://doi.org/10.5194/egusphere-2023-238
Preprint. Discussion started: 3 April 2023

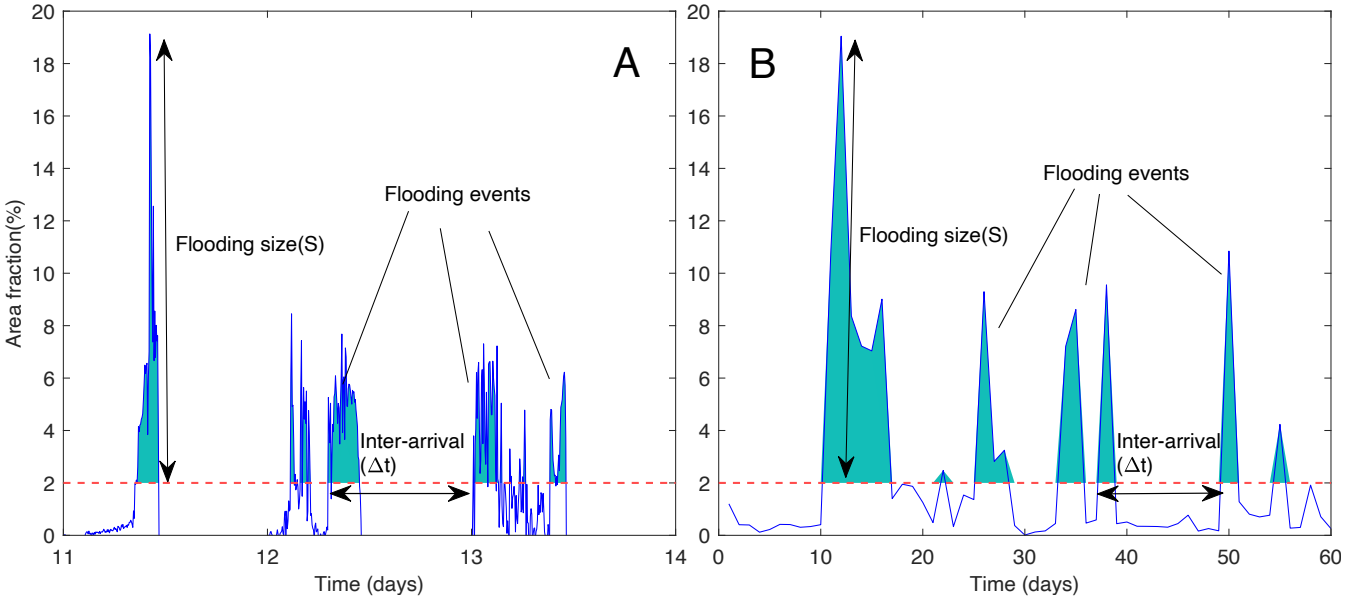

Figure 4. Definition of the flooding events, their size (S) and inter arrivals (Δt) from the excess water area fraction $A(t)$. Examples shown for the original timescale $\tau = 5$min (A), and for a daily timescale ($\tau = 1$day) (B).

the duration of the event (Fig. 4). Furthermore, we defined the inter-arrival time Δt_i as the time between consecutive flooding events $t_{i+1} - t_i$. Below, we analyze the probability distribution function of the duration d, size S and inter-arrival time Δt of flooding events at different timescales τ.

3 Statistical analysis of measured flooding events

3.1 Duration of flooding events

At the lowest timescale (and higher time resolution, $\tau = 5$ min), the probability density function $f(d)$ of the duration d of flooding events lasting up to 2 hours seems followed a power-law distribution (Fig. 5),

$$f(d) = \frac{\beta}{d_{\min}} \left(\frac{d_{\min}}{d} \right)^{1+\beta} \tag{1}$$

with minimum duration $d_{\min} = 3$ minutes and $\beta = 0.7$.

Above 2 hours, the data drastically deviated from the power-law distribution with no event lasting more than 3 hours, which suggested a physical upper-limit for sustained flooding conditions in the absence of a large storm, such as a hurricane.

Furthermore, the size and duration of flooding events was poorly correlated (Fig. 6), as events where water covered around 10% of the images' pixels (above normal coverage), i.e. $S > 10\%$, can lasted from 10 minutes to 2 hours. However, there was a lower temporal bound for the size of the events (Fig. 6)

https://doi.org/10.5194/egusphere-2023-238
Preprint. Discussion started: 3 April 2023

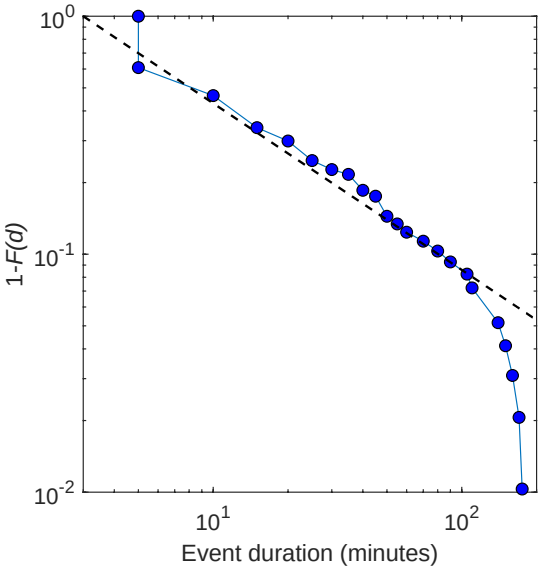

Figure 5. Complementary cumulative distribution function $1 - F(d)$ (F is the cumulative distribution function) of the duration d of flooding events. Line shows the power-law $(d_{\min}/d)^{\beta}$ with minimum duration $d_{\min} = 3$ min and exponent $\beta = 0.7$. The time resolution of the data sets a lower cutoff at $d = 5$min.

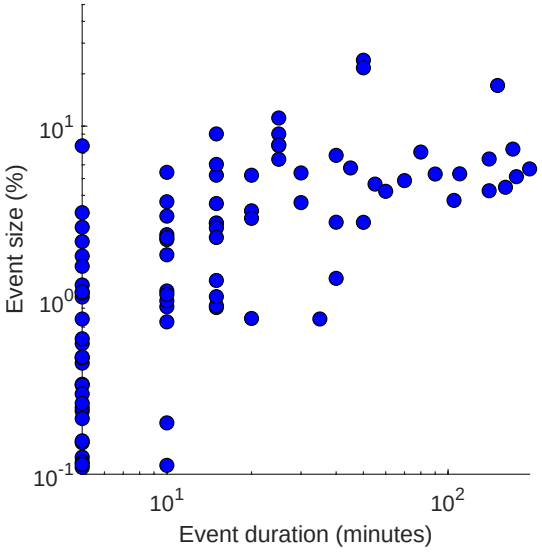

Figure 6. Relation between the size S and duration d of flooding events. Note that the time resolution of the data is 5 minutes.

https://doi.org/10.5194/egusphere-2023-238
Preprint. Discussion started: 3 April 2023

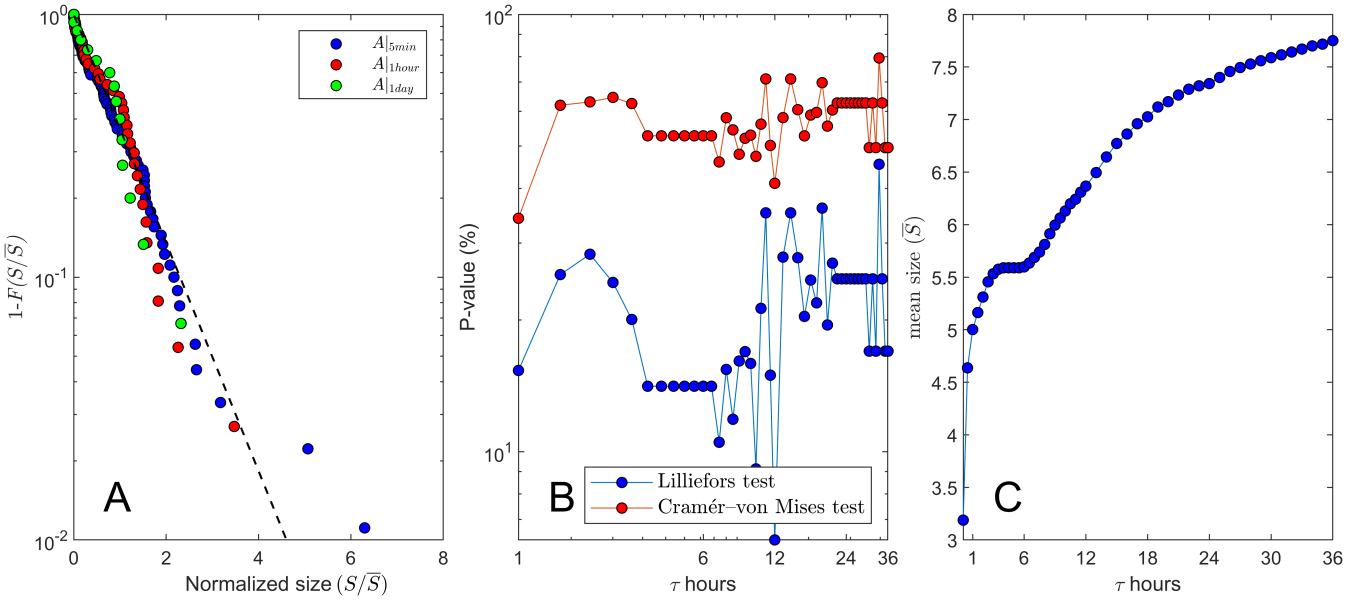

Figure 7. (A) Complementary cumulative distribution function $1 - F(S/\bar{S})$ of the flooding event size S normalized by the mean $\bar{S}$ at three different timescales: $\tau = 5$min, 1 hour and 1 day. The exponential distribution $e^{-S/\bar{S}}/\bar{S}$ is shown for reference. (B) P-values testing compatibility with the exponential distribution at different timescales (τ) — 0% (100%) indicate perfect incompatibility (compatibility) with 5% as the typical threshold for passing the test. (C) Average size $\bar{S}$ of flooding events (%) for different timescales τ.

3.2 Distribution of flooding size

The distribution of the size S of flooding events, obtained from the time series of water area at the lowest timescale ($\tau = 5$ min), was well approximated by the exponential distribution $e^{-S/\bar{S}}/\bar{S}$ (Fig. 7a), with an average flooding size $\bar{S} = 3.36\%$. The flooding size distribution remained exponential for timescales τ up to the maximum value investigated (1.5 days), with p-values higher than rejection range for both Lilliefors test (6.28 % to 45.4%) and Cramér-von Mises test (34.1% to 79.4 %), commonly used test for the exponential fit (Lilliefors, 1969; Cramér).

The exponential distribution of flooding size S agreed with findings by Rinaldo et al. (2021) for the size of beach overtopping events (referred to as high-water-events) obtained from the daily time series of total water levels. This agreement suggested that the distribution type was robust with respect to potential variations of the local beach slope during the measurement period and alongshore flooding variations at the spatial scale defined by the camera field-of-view.

3.3 Distribution of inter-arrivals

The distribution of inter-arrivals Δt strongly depended on the timescale τ and seemed to have converged towards an exponential distribution for timescales above ~ 10 hours (Fig.8A and B). This was evidenced by the sharp increase in the p-values of both

https://doi.org/10.5194/egusphere-2023-238
Preprint. Discussion started: 3 April 2023

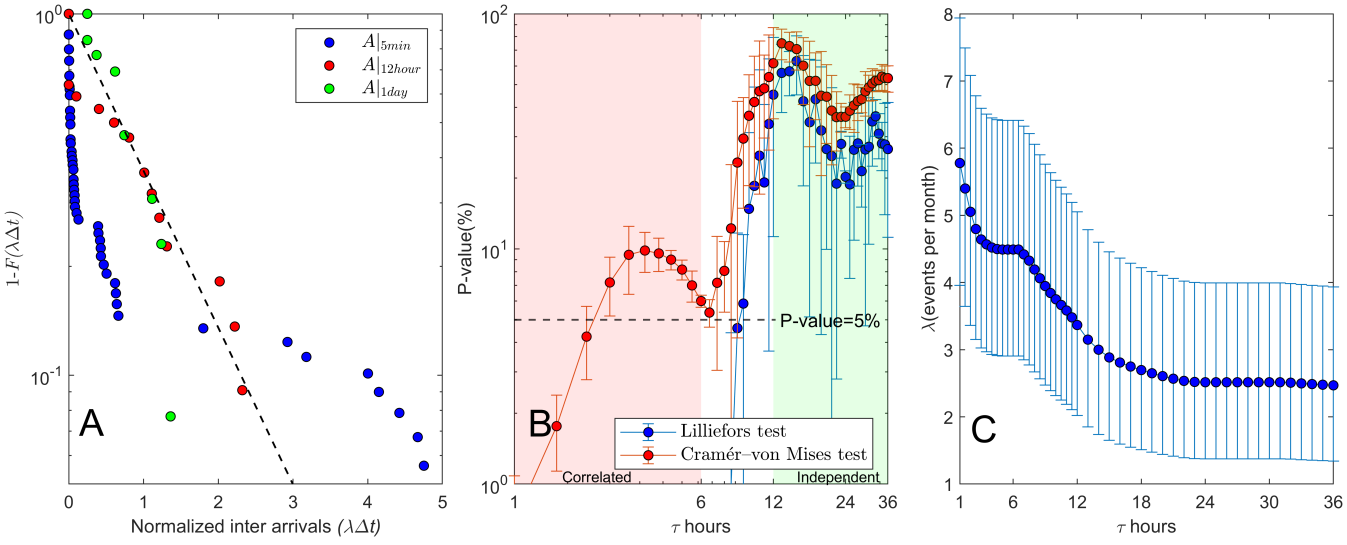

Figure 8. (A) Complementary cumulative distribution function $1 - F(\lambda\Delta t)$ of the inter arrivals (Δt) of flooding events normalized by the flooding frequency $\lambda = 1/\overline{\Delta t}$, at timescales τ =5 min, 12 hours and 1 day. The exponential distribution is shown for reference (dashed line). (B) Mean P-values with confidence bound ($\pm\sigma$) testing compatibility with the exponential distribution at different timescales (τ) — 0% (100%) indicate perfect incompatibility (compatibility) with 5% as the typical threshold for passing the test. Passing the test, i.e. inter-arrivals are exponentially distributed, means the events are independent, whereas failing the test suggests the events are correlated. (C) Frequency λ of flooding events at different timescales (τ), including the 95% confidence interval obtained by $\lambda \times [c_{\text{lower}}, c_{\text{upper}}]$, where $c_{\text{lower}} = \chi^2_{0.025,2n}/2n$, $c_{\text{upper}} = \chi^2_{0.975,2n}/2n$.

the Lilliefors and the Cramér-von Mises tests from around 10% to about 60% for timescales between 10 and 12 hours (Fig.8B). P-values remained above 30% for larger timescales.

In these statistical tests, the time at which the time-window analysis started was corrected for the time at which the time-window analysis starts. For a given timescale τ, we calculated the goodness of the exponential fit n times, where $n = \tau/5\text{min}$ is the number of every possible initial time at which the time-window of size τ could start. For example, the statistical tests were conducted only once for $A|5\text{min}(t)$, but 12 times for $A|1\text{h}(t)$ and 288 times for $A|_{1\text{d}}(t)$.

Given that the exponential distribution of inter-arrivals implied that the events were random and independent, indicating a Poisson process. We interpreted that the large deviations from the exponential distribution for timescales less than 10 hours as evidence of correlation between consecutive events (Fig. 8B). At larger timescales, consecutive flooding events seemed to have become independent and could be modelled as a Poisson process, in agreement with the findings of Rinaldo et al. (2021) for beach overtopping events. This change in temporal correlation seemed to be related to the timescale of local weather patterns affected by the daily cycle.

https://doi.org/10.5194/egusphere-2023-238
Preprint. Discussion started: 3 April 2023

3.4 Frequency of flooding events

The frequency λ of flooding events is by definition the inverse of the average inter-arrival $\lambda = 1/\overline{\Delta t}$ or equivalently $\lambda = N/T$, where N is the total number of flooding events obtained from $A|_\tau(t)$ and $T = 167$ days is the duration of the time series. As expected, λ decreased with the timescale τ as flooding events are merged, reached a plateau at the daily scale of 2.5 events per month, from about 6 events per month at the hourly scale (Fig. 8C). The decrease in λ mirrored the transition from correlated to uncorrelated events taking place for timescales between 6 to 12 hours (Fig. 8B).

4 Comparison with run-up model predictions

The stochastic model of flooding events measured over timescales exceeding 10 hours were in agreement with previous findings for high-water-events (HWEs) that cause overtopping of the beach, as stated in a previous section (Rinaldo et al., 2021). However, we sought to ask: Can the HWE predictions also match the measured flooding frequency from the camera observations, and, if so, are HWE predictions correlated with the measurements at the daily level?

According to Rinaldo et al. (2021), we obtained HWEs from the daily time series of total water levels defined as the sum of the still water level measured by the tidal gauge and a semi-empirical estimation of the 2%-exceedance wave run-up (Rinaldo et al., 2021). This semi-empirical estimation relied on off-shore data of significant wave height and peak wave frequency and the local beach slope (Stockdon et al., 2006, 2014). We used tidal gauge and buoy wave data in Galveston, Texas, the closest site. Rinaldo et al. (2021) already estimated the hourly time series of total water elevation for this site using a beach slope of 0.02 (Houser et al., 2015). For consistency, we removed total water levels during non-observation hours of flooding monitoring. We then converted the hourly time series of total water level to the daily maximum total water level, η_d, by sampling maximum values per each day. Finally, we defined the HWEs as the set of daily total water levels exceeding a given beach elevation threshold, Z_c.

Since flooding events and HWEs are equivalent for the purpose of this work, in what follows we will refer to HWEs as 'predicted flooding events', in contrast to the 'measured' flooding events obtained from our CNN-based analysis of camera observations.

Frequency of flooding events

As expected, the frequency of predicted flooding (from HWEs) decreased with beach elevation as the number of overtopping events decreased (Fig.9). The predicted flooding frequency was within the statistical range of the measurements for beach elevations between 0.5m and 0.9m. In particular, for the beach elevation of 0.7m, the predicted frequency matched the measured value of $\lambda = 2.5$ month^{-1} obtained for a daily timescale ($\tau = 24$h), as seen in Fig.8C. This beach elevation was noticeable lower than the characteristic beach elevation 0.9m estimated by Rinaldo et al. (2021) using a digital elevation model of the area (DEM, Fig. 9). However, it was consistent with the large observed beach erosion in our field site after hurricane Harvey in August 2017. Indeed, the beach scarp visible in Fig. 1, panel A_1, is about 20cm tall.

https://doi.org/10.5194/egusphere-2023-238
Preprint. Discussion started: 3 April 2023

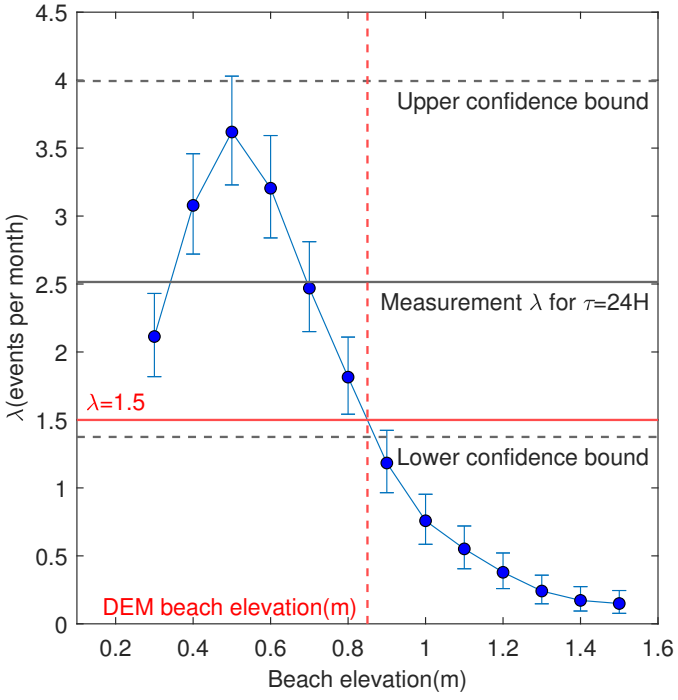

Figure 9. Frequency (λ) of high water events overtopping the beach, obtained from extrapolated water elevation data (Rinaldo et al., 2021), as function of the beach elevation. The measured flooding frequency extracted from the water area daily time series $A|_{1d}(t)$ (mean $\pm$ 95% confidence interval) is shown for comparison.

4.1 Synchronicity of measured and predicted flooding events

We compared the flooding predictions to the measurements at the daily level by defining a corrected and normalized daily time series of the measured flood area (R_m) and the predicted water elevation above the beach (R_p) as follows:

$$R_m(t) = \frac{A|_{1d}(t) - 2\%}{\overline{S_m}} \Theta(A|_{1d}(t) - 2\%) \quad (2)$$

$$R_p(t) = \frac{\eta_d(t) - Z_c}{\overline{S_p}} \Theta(\eta_d(t) - Z_c) \quad (3)$$

where, for the measurements , $A|_{1d}$ was the excess water area fraction at the daily timescale, 2% was the imposed threshold for flooding conditions. The mean size of the measured flooding events for $\tau = 24h$ was $\overline{S_m} = 7.5\%$(see Fig. 7C).

For the predictions, η_d was the estimated total water level at the shoreline, Z_c was the characteristic beach elevation and $\overline{S_p} = 0.3$m was the mean size of the predicted HWEs (Rinaldo et al., 2021). In both cases, $\Theta(x)$ is the step function (1 for $x > 0$ and 0 otherwise). Due to lack of data, we could only generate predictions for the first 130 days of our total 170 day measurement period (Fig. 10).

In spite of the numerous uncertainties in the estimation of the actual total water level from off-shore wave data and its application to estimate local run-up and beach overtopping, both time series were remarkably similar for the beach elevation

https://doi.org/10.5194/egusphere-2023-238
Preprint. Discussion started: 3 April 2023

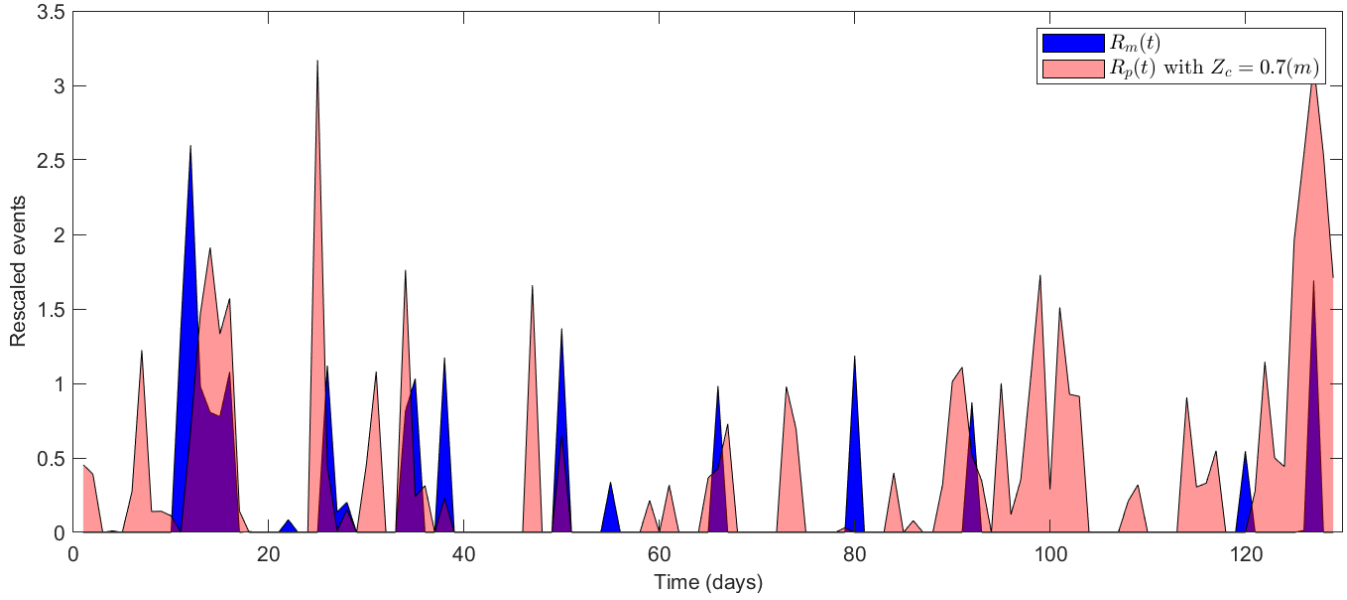

Figure 10. Corrected and normalized daily time series of measured flooded area (R_m) and predicted water elevation above the beach (R_p) from 23 Nov 2017 to 31 Mar 2018, when both time series are available (see definition in the main text). At the selected beach elevation ($Z_c = 0.7$m) the predicted flooding frequency from water elevation data equals the measured one from flooded area (see Fig. 9).

$Z_c = 0.7$m at which the predicted flooding frequency equals the measured one (Fig. 10). Indeed, most measured events were accurately captured by the prediction, including their relative intensity.

We evaluated the performance of the run-up model in predicting the measurements at the daily level using the conditional probabilities $P(m|p)$ and $P(p|m)$. The first one was the probability of measuring an event (m) that was predicted (p), and the second one was the probability of predicting an event (p) that was measured (m). Figure 11 shows the rates of false positives $1-P(m|p)$ and false negatives $1-P(p|m)$ of the prediction as function of beach elevation Z_c. As already apparent in Fig. 10, for $Z_c = 0.7$m, the rate of false negatives was relatively low $\sim 25\%$ whereas the rate of false positives was quite high $\sim 75\%$. As the beach elevation increased, the rate of false negatives drastically increased, which suggests that our estimation of the local beach elevation by comparing the predicted (using a run-up model) and measured (using our camera data) flooding frequencies is consistent with the daily time-series of total water elevation predicted from the run-up model (Fig. 10). However, no similar improvement occurred for the rate of false positives, as the run-up model consistently overpredicted flooding days at all beach elevations.

Given the nature of the run-up predictions using off-shore data (Stockdon et al., 2006, 2014), that in a first approximation neglects the alongshore variability of the bathymetry or the details of wave shoaling (García-Medina et al., 2017; Atkinson et al., 2017), one can argue that the prediction only indicates conditions favorable to flooding events somewhere along the shoreline and not necessarily the actual occurrence of a flooding event at a precise location. This statistical interpretation would be inline with our findings.

https://doi.org/10.5194/egusphere-2023-238
Preprint. Discussion started: 3 April 2023

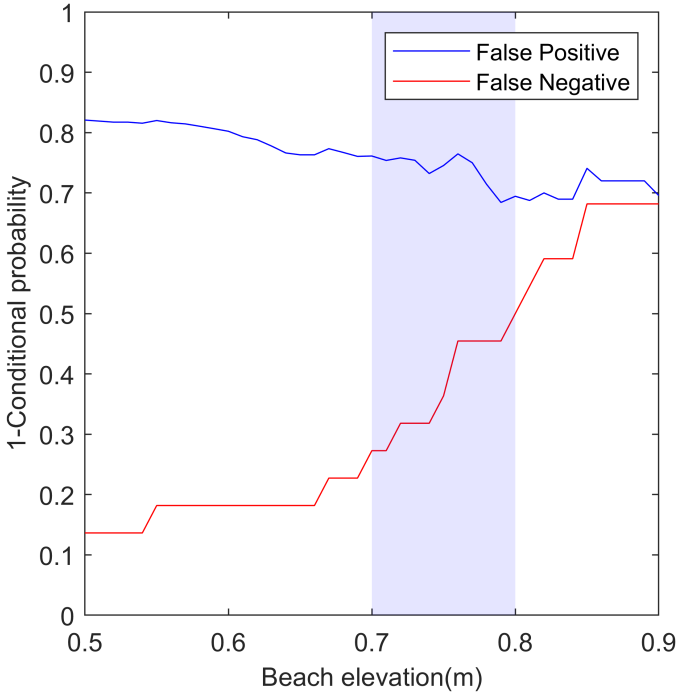

Figure 11. Performance of the model predictions when compared to the measurements. False positive and false negative rates are defined in terms of conditional probabilities as the probability of flooding predicted but not measured, and the probability of flooding measured but not predicted, respectively (see text for detailed definition).

5 Discussion and Conclusion

We studied the stochastic properties of coastal flooding events monitored via 5-minutes time-lapse imagery for more than 160 days and processed using CNN-based image segmentation. When analyzing the data at the daily timescale, we find flooding events can be modeled as a Poisson process with exponentially distributed sizes, in agreement with recent findings using a run-up model to predict beach overtopping (Rinaldo et al., 2021). The correlation between consecutive events depended on the timescale at which we defined the flooding events. Following our statistical analysis of event inter-arrivals, flooding events seems to be correlated for timescales smaller than 10 hours, while events are random and independent at larger timescales, thereby following a Poisson process.

The frequency of flooding events depended strongly on the timescale at which data was analyzed, and decreased from about 6 events per month at the hourly timescale to a plateau of 2.5 events per month at the daily timescale. Although this value is larger than the frequency of 1.5 events per month predicted by HWEs (Rinaldo et al., 2021) for natural beaches, the latter value was within the confidence bounds of our data, which were relatively large due to the short time period analyzed. Nevertheless, a higher measured flooding frequency was expected because of beach erosion induced by hurricane Harvey.

https://doi.org/10.5194/egusphere-2023-238
Preprint. Discussion started: 3 April 2023

We found the size of flooding events was exponentially distributed with average sizes of about 4% of the camera field-of-view when data was analyzed at the hourly timescale to a maximum 8% at the daily or-larger timescale. When estimated at the highest 5-minute resolution, we also found the actual duration of flooding events typically varies between 10 and 100 minutes, and seemed to follow a power-law distribution. However, there was a poor correlation between the size and the duration of flooding events.

Finally, at the daily timescale, we found the runup model behind the HWEs prediction of Rinaldo et al. (2021) indeed captures the occurrence of local flooding, although it noticeably overpredicts them. Furthermore, we found a good agreement between the predicted flooding frequency (from HWEs) and our measurements when taking into account local beach erosion due to hurricane Harvey.

In summary, by validating the predictions of Rinaldo et al. (2021), our work demonstrates the suitability of HWEs predictions based on relatively simple run-up models to estimate the frequency and intensity of beach and dune overtopping. We also provided a detailed characterization of the probabilistic structure of flooding events, including its frequency, intensity and duration. Our results thus formalize, i.e. validate and expands, the first probabilistic model of coastal flooding events driven by wave run-up. After further estimation of the model parameters for different locations, this probabilistic model can be used in coastal risk management and landscape evolution models.

Author contributions. O.D.V. designed the study. O.D.V., R.A.F. and T.H. installed the field equipment and carried out the observations. B.K. performed the time series analysis. B.K and O.D.V. performed the probabilistic analysis. B.K and O.D.V. prepared the manuscript with contributions from all co-authors.

Competing interests. The authors declare that they have no conflict of interest.

Acknowledgements. O.D.V. and B.K were supported by the Texas A&M Engineering Experiment Station.

https://doi.org/10.5194/egusphere-2023-238
Preprint. Discussion started: 3 April 2023

References

Atkinson, A. L., Power, H. E., Moura, T., Hammond, T., Callaghan, D. P., and Baldock, T. E.: Assessment of runup predictions by empirical models on non-truncated beaches on the south-east Australian coast, Coastal Engineering, 119, 15–31, https://doi.org/https://doi.org/10.1016/j.coastaleng.2016.10.001, 2017.

Bevacqua, E., Maraun, D., Vousdoukas, M. I., Voukouvalas, E., Vrac, M., Mentaschi, L., and Widmann, M.: Higher probability of compound flooding from precipitation and storm surge in Europe under anthropogenic climate change, Science Advances, 5, eaaw5531, https://doi.org/10.1126/sciadv.aaw5531, 2019.

Cramér, H.: On the composition of elementary errors, Scandinavian Actuarial Journal, 1928, 141.

Durán Vinent, O., Schaffer, B. E., and Rodriguez-Iturbe, I.: Stochastic dynamics of barrier island elevation, 118, e2013349 118, https://doi.org/10.1073/pnas.2013349118, 2021.

García-Medina, G., Özkan-Haller, H. T., Holman, R. A., and Ruggiero, P.: Large runup controls on a gently sloping dissipative beach, Journal of Geophysical Research: Oceans, 122, 5998–6010, https://doi.org/10.1002/2017jc012862, 2017.

Houser, C., Wernette, P., Rentschlar, E., Jones, H., Hammond, B., and Trimble, S.: Post-storm beach and dune recovery: Implications for barrier island resilience, Geomorphology, 234, 54–63, https://doi.org/https://doi.org/10.1016/j.geomorph.2014.12.044, 2015.

Kang, B., Feagin, R. A., Huff, T., and Duran Vinent, O.: Stochastic properties of coastal flooding events - Part 1: CNN-based semantic segmentation for water detection, Earth Surface Dynamics, in review.

Kriebel David, L. and Dean Robert, G.: Convolution Method for Time-Dependent Beach-Profile Response, Journal of Waterway, Port, Coastal, and Ocean Engineering, 119, 204–226, https://doi.org/10.1061/(ASCE)0733-950X(1993)119:2(204), 1993.

Lilliefors, H. W.: On the Kolmogorov-Smirnov Test for the Exponential Distribution with Mean Unknown, Journal of the American Statistical Association, 64, 387–389, https://doi.org/10.2307/2283748, 1969.

Moftakhari, H. R., Aghakouchak, A., Sanders, B. F., Allaire, M., and Matthew, R. A.: What Is Nuisance Flooding? Defining and Monitoring an Emerging Challenge, Water Resources Research, 54, 4218–4227, https://doi.org/10.1029/2018wr022828, 2018.

Muis, S., Verlaan, M., Winsemius, H. C., Aerts, J. C. J. H., and Ward, P. J.: A global reanalysis of storm surges and extreme sea levels, Nature Communications, 7, 11 969, https://doi.org/10.1038/ncomms11969, 2016.

Rinaldo, T., Ramakrishnan, K. A., Rodriguez-Iturbe, I., and Durán Vinent, O.: Probabilistic structure of events controlling the after-storm recovery of coastal dunes, Proceedings of the National Academy of Sciences, 118, e2013254 118, https://doi.org/10.1073/pnas.2013254118, 2021.

Stockdon, H. F., Holman, R. A., Howd, P. A., and Sallenger, A. H.: Empirical parameterization of setup, swash, and runup, Coastal Engineering, 53, 573–588, https://doi.org/https://doi.org/10.1016/j.coastaleng.2005.12.005, 2006.

Stockdon, H. F., Thompson, D. M., Plant, N. G., and Long, J. W.: Evaluation of wave runup predictions from numerical and parametric models, Coastal Engineering, 92, 1–11, https://doi.org/https://doi.org/10.1016/j.coastaleng.2014.06.004, 2014.

Ward, P. J., Couasnon, A., Eilander, D., Haigh, I. D., Hendry, A., Muis, S., Veldkamp, T. I. E., Winsemius, H. C., and Wahl, T.: Dependence between high sea-level and high river discharge increases flood hazard in global deltas and estuaries, Environmental Research Letters, 13, 084 012, https://doi.org/10.1088/1748-9326/aad400, 2018.